ISTITUTO NAZIONALE DI GEOFISICA E VULCANOLOGIA

Monitoring the time-averaged discharge rates, volumes and emplacement style of large lava flows by using MIROVA system: the case of the 2014-2015 eruption at Holuhraun (Iceland)

D. Coppola[1][2] S. Barsotti[3], C. Cigolini[1][2], G., M. Laiolo[1][4], M.A., Pfeffer[3], M. Ripepe[4]

(1) Dipartimento di Scienze della Terra, Universita di Torino, Via Valperga Caluso 35, 10125 Turin, Italy

(2) NatRisk, Centro Interdipartimentale sui Rischi Naturali in Ambiente Montano e Collinare, Universita` degli Studi di Torino, Italy

(3) Icelandic Meteorological Office. Bustaðavegi 7- 9, 108 Reykjavik, Iceland

(4) Dipartimento di Scienze della Terra – Universita di Firenze. Via G. La Pira 4, 50121 Florence, Italy.

Monitoring the time-averaged discharge rates, volumes and emplacement style of large lava flows by using MIROVA system: the case of the 2014-2015 eruption at Holuhraun (Iceland)

D. Coppola[(1)(2)], S. Barsotti[(3)], C. Cigolini[(1)(2)], G., M. Laiolo[(1)(4)], M.A., Pfeffer[(3)], M. Ripepe[(4)]

Corresponding author: Coppola Diego (diego.coppola@unito.it).

(1) Dipartimento di Scienze della Terra, Università di Torino, Via Valperga Caluso 35, 10125 Turin, Italy

(2) NatRisk, Centro Interdipartimentale sui Rischi Naturali in Ambiente Montano e Collinare, Universita` degli Studi di Torino, Italy

(3) Icelandic Meteorological Office. Bústaðavegi 7- 9, 108 Reykjavík, Iceland

(4) Dipartimento di Scienze della Terra – Università di Firenze. Via G. La Pira 4, 50121 Florence, Italy.

Abstract

The 2014-2015 eruption at Holuhraun has produced more than 1.5 km^3 of basaltic magma and can be considered one of the major effusive events of the last two centuries in the world. During this eruption the MIROVA system (a volcanic hot-spot detection system based on MODIS middle infrared – MIR - data) has been used to detect and locate the active portions of the lava flow(s), and to measure the heat radiated by the growing lava field. According to these data the eruption was characterized by a slow decay of the radiant power, accompanied by a change in the lava transport mechanism that shifted from open channels, at the beginning of the eruption, to lava tubes, during the last months of activity. Despite the evident evolution of lava transport mechanism, we found that the overall decreasing trend of the thermal flux was mainly controlled by the exponential decline of lava discharge rates, while the increasing insulation of the flow field had a strong impact in transporting efficiently the lava at the distal flow front(s). Our results suggest the apparent time averaged lava discharge rates (*TADR*), derived from satellite thermal data, may fluctuate around the real effusion rate at the vent, especially in the case of large lava flows emplacing in nearly flat conditions. The magnitude and frequency of these fluctuations are mainly controlled by the emplacement dynamic, (i.e. occurrence of distinct major flow units), while the transition from channel- to tube-fed lava transport mechanism play only a minor role (±30%) in the retrieval of *TADR* using MIR data . When the *TADR* values are integrated to calculate erupted lava volumes, the effects of pulsating emplacement dynamic become smoothed and the eruptive trend become more clear.

We suggest that during the Holuhraun's eruption, as well as during many other effusive eruptions, the MIR-derived radiant flux essentially mimic the overall trend of lava discharge rates, with only a minor influence due to the emplacement style and evolving eruptive conditions. From a monitoring and operational perspective, MIROVA demonstrates to be a very valuable tool to follow and, possibly, forecast the evolution of on-going effusive eruptions.

1. Introduction

On August 29th 2014, one of the largest effusive eruption of the last 3 centuries took place along the Eastern Volcanic Zone (EVZ) of Iceland, about 45 km north-east of Bárðarbunga volcanic system (Gudmunsson, et al., 2014). The new eruption followed 15 days of sustained seismicity and accompanied the propagation of a 45 km long dike (Sigmundsson et al., 2015) that unlocked an historical eruptive path named Holuhraun (Sigurðsson and Sparks, 1978). The emission of lava persisted at very high rate for 180 days up to February 27th, 2015 when the activity was declared over (Gislason et al., 2015). The eruption was characterized by a slow decay of effusion rate (Coppola et al., 2017) that accompanied a coeval slow subsidence of the Bárðarbunga caldera (Gudmundsson et al., 2016). The clear link between the two processes provided evidences of an inelastic eruption whereby the lateral magma withdrawal was essentially linked to the gravity-driven collapse of the summit caldera (Coppola et al., 2017, Gudmundsson et al. 2016). About 84 km^2 of nearly flat land was covered by the new lava field that reached a maximum extend of about 18 x 5 km (Figure 1) and thickness up to 40 m (Gislason et al., 2015, Pedersen et al. 2017).

The prohibitive environmental conditions that might characterize these latitudes made field observations at the eruptive site very hard, especially on a continuous basis and for several months during the winter time. In these conditions, space-based thermal data have been extremely useful since they allowed a safe detection, location and quantification of the radiant flux produced by the effusive activity. In particular, infrared data acquired by MODIS (Moderate Resolution Imaging Spectroradiometer) and elaborated through the MIROVA volcanic hotspot detection system, (Coppola et al., 2016; www.mirovaweb.it), were delivered to the Icelandic Meteorological Office (IMO) as part of its daily operational monitoring activity of the Holuhraun eruption.

Since the beginning of the eruption the main tasks of satellite thermal data were: (i) to provide information about the location of active lava flow areas and front, (ii) to give an estimation of lava discharge rates and erupted volumes and finally (iii) to identify the ongoing effusive trend (steady,

waning or waxing). The latest two points became a priority after a couple of months when the winter

season and the low-light conditions made the eruptive site hardly accessible and field observations

became more and more rare and difficult. The calculation of effusion rates from satellite thermal data

(the so called "thermal proxy"), become one of the main topic discussion among a thermal remote

sensing group, established in that occasion by Dr. Thor Thordarson (Harris et al., 2016a). One of the

main questions discussed within the group was "whether the subtle, but persistent decay of thermal

flux indicated by satellite measurements, was caused by a real, slow decline of the effusion rate or

reflected the increasing insulation of the growing lava field and the development of a lava tube system

(Pedersen et al., 2017)
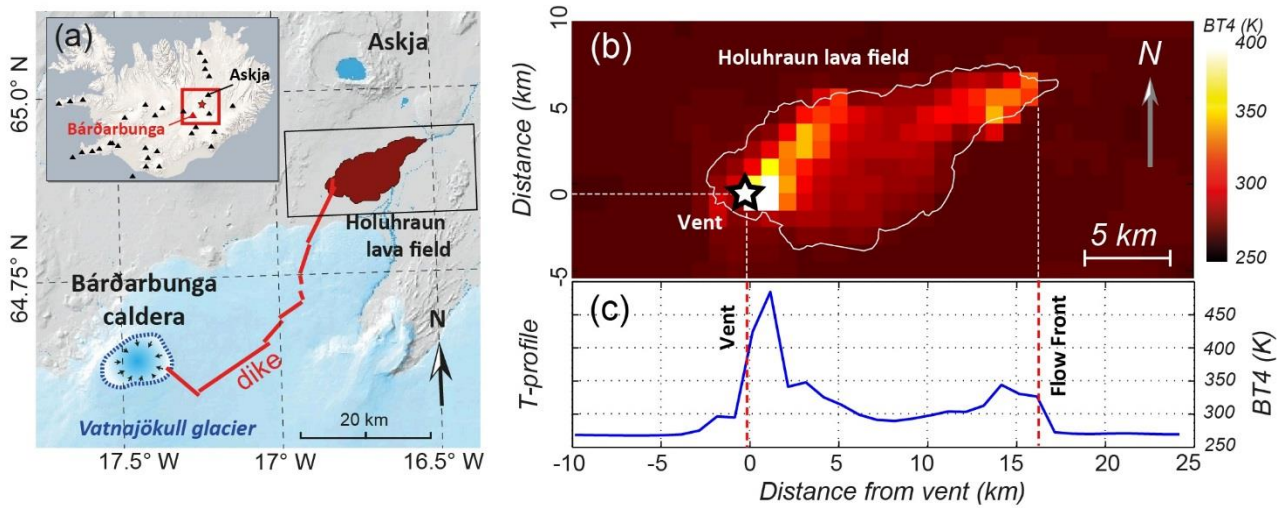
Figure 1. (a) Location of the Bárðarbunga-Holuhraun volcanic system showing the ice covered, 10-km-wide caldera of
Bárðarbunga and the 2014-2015 lava filed at Holuhraun. (b) Example of MODIS-derived thermal image (spatial
resolution of 1 km) showing the Brightness Temperature at 4 μm (BT4) recorded on February 03rd, 2015 over the
Holuhraun lava field (white line). The star indicates the approximate location of the vent. (c) Temperature profile along
W-E direction, obtained by calculating the maximum BT4 along each vertical (N-S) line. The position of the flow front
is marked by the easternmost thermally anomalous pixel (see the text for details).

In this paper we present time-averaged lava discharge rates and volumes, derived by using MIROVA system, and we compare the results with field and independent measurements collected during and after the Holuhraun eruption. The comparison reveals the role of changing emplacement style in the lava discharge rates calculation and outlines the contribution of MIROVA in safely tracking this large effusive eruptions from space.

2. Time-averaged discharge rates from satellite thermal data: background and open questions

The relationship between effusion rates and thermal emissions of lava flows has received increasingly attention during the past three decades (a full list of 46 papers published between 1990 and 2005 is reported in Harris 2013). The methods, limits and applications of this approach are part of a book expressly focussed on detecting, modelling and responding to effusive eruptions (Harris et al., 2016b), whereas exhaustive overview of the physic behind mass and energy flow through a lava flow system is provided by a series topical works (Pieri and Baloga 1986, Crisp and Baloga 1990, Harris et al., 1997, Wright et al., 2001, Harris et al., 2007, Harris and Baloga 2009; Dragoni and Tallarico 2009, Coppola et al, 2013; Garel et al., 2012, 2014, 2015, Tarquini (2017), among others). Here, we outline the basic principles of this technique and we summarize the open questions that have been addressed in this work.

To describe volumetric flow rates of erupted lavas, we use the terminology given by Harris et al. (2007). We use the generic term *effusion rate*, to describe the instantaneous rate at which lava is erupted from the vent at any time. The term *mean output rate* (*MOR*) is used to describe the final volume of erupted lava divided by the total duration of the eruption. Finally, we used the term *time-averaged lava discharge rate* (*TADR*) to describe the volume of lava emplaced during a specific time interval (Harris et al., 2007). This definition better applies to the use of satellite-based methods, for

119 measuring the changes in lava volume over a given period of time prior the image acquisition (Wright

120 et al., 2001).

121 Currently, two main methods exist to estimate *TADRs* from space-based thermal data; the method of

122 Harris et al. (1997), simplified later by Wright et al. (2001), and the method of Coppola et al., (2013).

123 Both the methods rely on the original heat balance approach (Pieri and Baloga, 1986), stating that the

124 *mean output rate MOR* (m^3 s^{-1}) of a cooling-limited lava flow, is related to its final plan area *A*

125 (attained when the flow achieves its final length, *L*), by:

126

127 $$MOR = \frac{\varepsilon \sigma T_e^4}{\rho C_p (T_0 - T_{stop})} A(L) \qquad \text{(eq. 1)}$$

128

129 where ρ (kg m^{-3}) and C_p (J kg^{-1} K^{-1}) are the bulk density and heat specific capacity of lava,

130 respectively, T_e (K) is the effective radiation temperature of the flow, T_0 (K) is the lava eruption

131 temperature, and T_{stop} (K) is the temperature of the flow front at the time the flow has cooled to a halt.

132 In this framework, the effective radiation temperature is defined as "the temperature at which the flow

133 would radiate if it had a constant surface temperature throughout the emplacement of the flow" (Crisp

134 and Baloga, 1990).

135 Harris et al., (1997), applied this approach to satellite thermal data, developing what is actually called

136 the "thermal proxy". Further works (Wright et al., 2001; Harris et al. 2007, 2009) refined and

137 simplified this method suggesting that the equation 1, when applied to satellite radiance data, provides

138 discharge rates that are not necessarily averaged over the total duration of an eruption, but rather over

139 "some time" prior to the satellite acquisition. Here, the effective radiation temperature, T_e, takes a

140 specific meaning, since it represents the average surface temperature over "some time" prior to the

141 satellite acquisition, weighted according to the radiative heat flux (Harris and Baloga, 2009).

142 Accordingly, Harris et al., (2007) proposed to use the term "*time-averaged discharge rate*" (TADR),

143 in order to describe the discrete measurements of lava flux retrieved from single satellite thermal

144   images. Wright et al., (2001) also argued that all values except *MOR (or TADR)* and *A* are assumed

145   a priori in equation 1 so that the thermal proxy reduces to a simple relationship whereby:

146

147    $TADR = Ax$ (eq. 2)

148

149   Here x is an empirical parameter (m s^{-1}), that describes the appropriate compositional flow parameters

150   (ρ, C_p) as well as thermal insulation (T_e) and cooling (T_0-T_{stop}) conditions (cf. Harris and Baloga

151   2009). In this formulation the area of the active flow area, A (m^2) is also dependent on the insulation

152   condition expressed by T_e, and is directly retrieved from the pixel integrated spectral radiance, R_λ (W

153   m^{-2} sr^{-1} µm^{-1}), according to:

154

155    $$A = \sum_{i=1}^{npix} \frac{R_\lambda - L_\lambda(T_{bk})}{L_\lambda(T_e) - T_\lambda(T_{bk})} A_{pixel}$$ (eq. 3)

156

157   where T_{bk} is the background temperature (K), L_λ is the Plank function for wavelength λ (W m^{-2} sr^{-1}

158   µm^{-1}), and A_{pixel} is pixel area (1 km^2 for MODIS). By assuming two end-member radiating

159   temperatures (T_e) for the hot and cold models (for example 500°C and 100°C for the channel- and

160   tube-fed flow type, respectively), the equation 3 allows the user to calculate a range of plausible active

161   flow areas, responsible for the observed radiance (Harris et al., 2007).

162   As stressed by Harris and Baloga (2009), the values for x have to be set on a case-by-case, thus leaving

163   a wide arbitrariness to the user that may adjust all the unknowns in equation (1) to achieve a best-fit

164   with available and independent field data. The TIR (thermal infrared) bands are generally used in this

165   approach under the assumption that the surface area of high temperature cracks is small and provides

166   a negligible contribution to the pixel integrated radiance at 10 µm to 12 µm (Harris and Baloga 2009).

167 This approach (equations 2 and 3) was the one used by Bonny et al., (2018) to estimate the volume

168 of lava erupted during the 2014-2015 eruption at Holuhraun by using MODIS TIR data.

169

170 The method of Coppola et al., 2013, does not hold with the calculation of active flow areas, but is

171 based on the empirical relationship that directly links the $TADR$ with the Volcanic Radiant Power

172 (VRP) calculated via the MIR method (Wooster et al., 2003). The MIR-derived VRP is a measurement

173 of the heat flux radiated almost exclusively by the portions of lava flows having effective temperature

174 (T_e) above 600 K, and is calculated as:

175

176 $$VRP = 18.9 \cdot A_{pixel} \cdot \sum_{i=1}^{npix} \left(R_{MIR,alert} - R_{MIR,bk} \right)_i \qquad \text{(eq. 4)}$$

177

178 where $R_{MIR,alert}$ is the pixel integrated MIR radiance of the ith alerted pixel, $R_{MIR,bk}$ is the MIR radiance

179 of the background, A_{pixel} is the pixel size (1 km^2 for the resampled MODIS pixels), and 18.9 is a

180 constant of proportionality (see Wooster et al., 2003). The $TADR$ is than calculated by using a single

181 coefficient called radiant density (c_{rad} in in J m^{-3}):

182

183 $$TADR = \frac{VRP}{c_{rad}} \qquad \text{(eq. 5)}$$

184

185 that describes the relationship between volumetric and radiant flux appropriate for the observed

186 eruption (Coppola et al., 2013). By analyzing a large compositional spectrum of recent lava flows,

187 Coppola et al., (2013) proposed an empirical method to calculate the c_{rad}, based on the silica content

188 of the erupted lavas:

189

190 $$c_{rad} = 6.45 \times 10^{25} \times \left(X_{SiO_2} \right)^{-10.4} \qquad \text{(eq. 6)}$$

191 where X_{SiO2} is the silica content of the erupted lavas (wt%).

192 This method allows to take into account the strong effects that the bulk rheology has on the spreading

193 and cooling processes of active lavas, and, according to the authors, permit to estimates *TADR* with

194 an uncertainty of ± 50% (Coppola et al., 2013). Most importantly, it allows to calculate the appropriate

195 radiant density, once the first chemical analysis of the erupted lavas become available (Coppola et

196 al., 2017). Since the MIROVA system provides automatically the *VRP* (Coppola et al., 2016), the

197 radiant density approach (equations 5 and 6) was the one used by Coppola et al., 2017 to estimate

198 *TADR* and erupted lava volume during the Holuhraun eruption.

199

200 Although the two methods derive from the original heat balance approach, valid for cooling-limited

201 lava flows (eq. 1), it is important to remark that they do not necessarily yield exactly the same results

202 (cf. Bonny et al., 2018, Coppola et al., 2017). This is because the wavelengths used by the two

203 methods are different (R_{TIR} and R_{MIR}, respectively) but also because of the arbitrariness of the input

204 coefficients, as *x* for the Harris' method and c_{rad} for the Coppola's method. Nevertheless, both the

205 methods provide an upper and lower boundary estimates of *TADR* that are *linearly* related to the

206 pixel-integrated spectral radiances (cf. eq. 1 to 5). It follows that whatever the method used, a constant

207 *TADR* would be translated into a constant radiance detected by space.

208 This point was challenged by recent laboratory experiments and physical modelling of cooling

209 viscous gravity currents (Garel et al., 2012, 2014, 2015) according to which for a given magma

210 discharge rate the heat radiated by the flow surface reaches a steady value only after a transient time.

211 According to the cooling-limited flow model (eq. 1), this transient time would correspond to the time

212 required for the lava flow front to reach its maximum length (*L*) and to cool to a halt ($T_{front} = T_{stop}$).

213 Hence, during rapid changes of effusion rates the thermal signal would be "buffered" in time, because

214 it takes time for the higher flow rate to propagate downstream and cause perceptible increases in flow

215 area (Harris and Baloga 2009). The transient time thus reflect the dynamic response of the thermal

216 structure toward the appropriate cooling-limited conditions expressed by the new *TADR* vs. *A*

relationship (i.e. new steady-state condition). Tarquini (2017) also suggests that this transient time is typical of non-equilibrium steady-state systems, and is related to a structural relaxation time that operate particularly on long-lived lava flows. In this non-equilibrium framework, the active lava flow units represent "dissipative structures" that promote significant fluctuations in the radiative power, even in the case of a constant supply. Hence, the radiant flux would be modulated by a pulsating emplacement dynamic, associated to the occurrence of flow diversions that resets the system further from its maximum extension (cf. Tarquini 2017).

Other open questions remain challenging, especially for operational use of the thermal proxy during effusive crisis. For example, based on its theoretical model, Garel et al. (2012) suggests that when lava tubes form, the surface thermal signal will not reflect the flow dynamics, because the low crust temperatures do not reflect a potentially high flow rate of hot lava underneath. According to the authors, this would pose a serious problem, since many lava flows exhibit evolving emplacement styles throughout the eruption, often characterized by increasing insulation conditions and gradual formation of lava tubes. Similarly, it is still unclear how to determine whether an eruption has ceased based on thermal data, or whether the lava stored underneath a cooled crust can potentially emerge suddenly and spread rapidly (Garel et al., 2015). In these terms the 2014-2015 eruption at Holuhraun represents a key-case since allowed us to address all these points over the largest effusive eruptions occurred in the past three centuries.

3. Methods: Analysis of MODIS-MIR data

3.1 The MIROVA system

MIROVA (Middle Infrared Observation of Volcanic Activity) is an automated global hot spot detection system (www.mirovaweb.it) based on near-real time processing of Moderate Resolution Imaging Spectroradiometer (MODIS) infrared data (Coppola et al. 2016). The system completes automatic detection and location of thermal anomalies, and provides a quantification of the Volcanic

242 Radiative Power (*VRP*), within 1 to 4 hours of each satellite overpass. This is achieved through a

243 hybrid algorithm (fully described in Coppola et al., 2016) based on MIR radiance data (~ 4 μm)

244 recorded at 1-km spatial resolution, as shown in Fig. 1b. Two MODIS instruments (carried on two

245 NASA's satellites: Terra and Aqua) deliver approximately 4 images per day for every target volcano

246 located at equatorial latitudes. However, due to the polar, sun-synchronous orbit, the two satellites

247 increase their sampling time at high latitudes, providing, at least 6 to 10 overpasses per day over

248 Iceland. An example of thermal images elaborated by the MIROVA system during the Holuhraun

249 eruption is given in Fig. 1b.

250

251 *3.2 Volcanic radiative power and energy of the 2014-2015 eruption at Holuhraun*

252 Between August 29th, 2014 and March 4th, 2015, MIROVA detected hotspots in 1105 images over a

253 total of 1623 MODIS overpasses above Iceland (~68.1%). The volcanic radiative power (*VRP*) ranged

254 from ~39.1 GW, during the initial stage of the effusion, to less than 10 MW just before the end of the

255 eruption (Figure 2a). During the course of the eruption, we visually inspected all the acquired scenes

256 and we identified a large number of images acquired in cloudy conditions, and/or under poor

257 geometrical conditions that strongly deformed and affected the thermal anomaly at ground level.

258 These images were discarded from further analysis (blue circles in Fig. 2a) so that a supervised dataset

259 of only 206 high-quality images (~12.7% of the total MODIS overpasses) was used to provide a

260 robust quantification of *VRP* produced by the eruption (red circles in Fig. 2a). As a whole we

261 estimated that the Holuhraun eruption radiated approximately 1.6×10^{17} J into the atmosphere (red

262 curve in Fig. 2b), with a time-averaged radiant flux of about 10.5 GW.

263

264
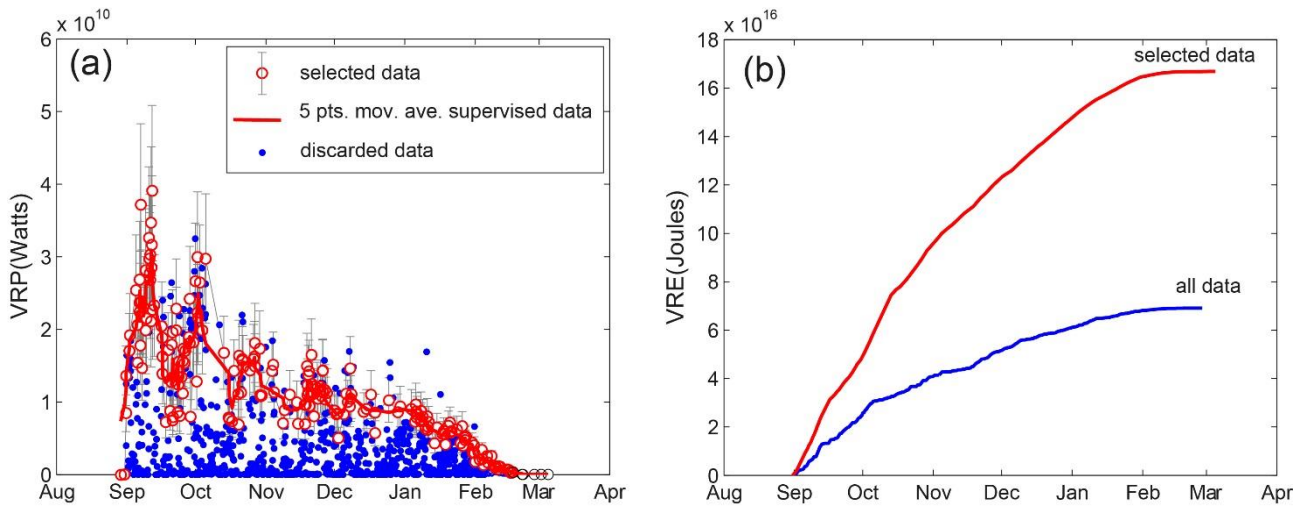
Figure 2. (a) Timeseries of *VRP* retrieved from MODIS-MIROVA system during the 2014-2015 eruption at Holuhraun.

Blue circles represent data discarded because of cloudy conditions or poor viewing geometry. The data selected for *VPR*

calculation are the white circles. The red line is a 5-points-moving average of *VRP*. A *VRP* below 10 MW coincides with

the end of the eruption. (b) Volcanic Radiative Energy (*VRE*) calculated by trapezoidal integration of selected data only

(red curve) or all the data (blue curve). Note the strong influence of data selection on the final total energy. Approximately

1.6×10^{17} J were radiated into the atmosphere (red curve), with a mean radiant flux of about 10.5 GW.

3.3 Time-averaged discharge rates and volume calculation

During the course of the eruption, we calculated *TADRs* and erupted lava volumes by using the radiant

density approach described above (eq. 5 and 6). The preliminary chemical analysis of Holuhraun

lavas (SiO_2 = 50.5 wt%), provided in early September 2014 by the University of Iceland

(http://earthice.hi.is/bardarbunga_2014), were used to calculate (eq. 6) a radiant density comprised

between 0.62×10^8 and 1.86×10^8 J m^{-3}. These two values allowed us to provide an upper and lower

boundary limits for lava volume calculation, with the mean value being the most likely (Fig. 3a).

Given a final *VRE* equal to 1.64×10^{17} J (Fig. 2b), this method provided a first, timely assessment of

the erupted lava volume equal to 1.75 ± 0.88 km^3 (Fig. 3a). This was in good agreement with the flow

volume estimated a-posteriori ($1.4 - 1.6$ km^3) by using independent datasets (Gislason et al. 2015,

Gudmundsson et al., 2016, Dirshel and Rossi, 2018; Bonny et al., 2018). The inferred satellite-

12

283 derived *TADR* and erupted volumes were updated continuously and delivered via emails to the teams

284 of the IMO and University of Iceland in charge of the monitoring.

285
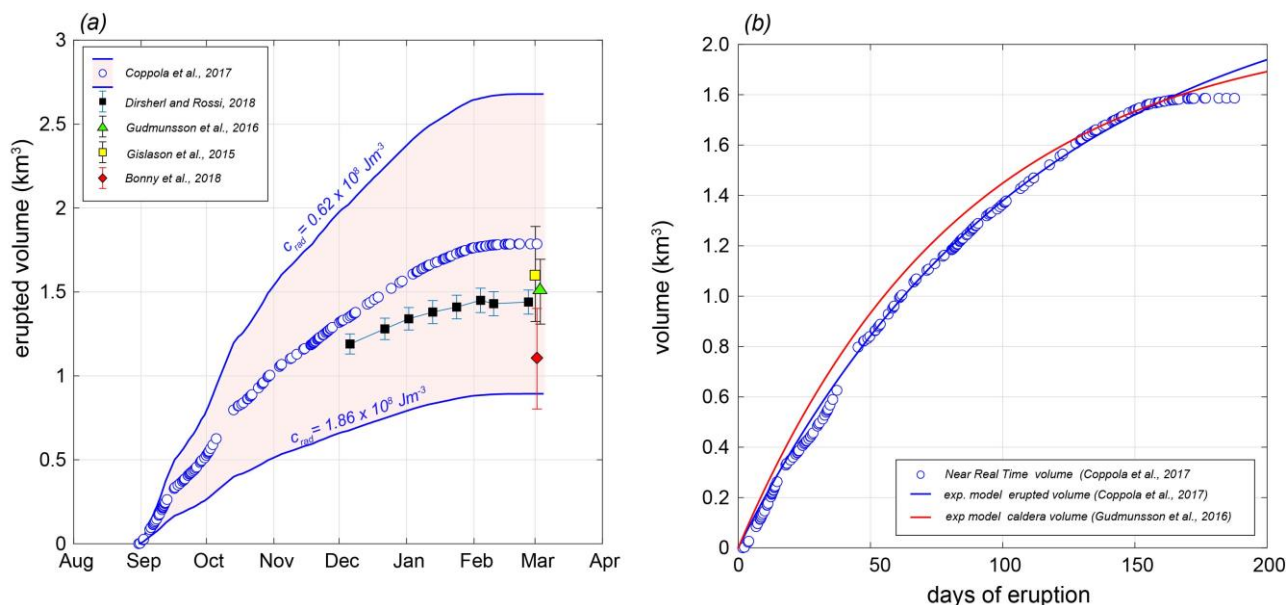
286

287 **Figure 3.** (a) Lava volumes measured during the 2014-2015 eruption at Holuhraun. The colored field envelop the upper

288 and lower boundary limits calculated using the radiant density approach (eqs. 5 and 6). Best-estimate volume calculation

289 (blue circles), and relative uncertainty (±50%) were provided in near real time to IMO and University of Iceland.

290 Independent measurements of final lava flow volumes given by several authors are also shown. (b) Comparison between

291 lava field volume measured by MODIS (blue circles) and exponential models of erupted lava volume (Coppola et al.,

292 2017) and caldera volume (Gudmunsson et al., 2016). The good correlation indicates a strong link between to the gravity-

293 driven collapse of Bárðarbunga caldera and the gradual decrease of magma-static pressure driving the effusive eruption

294 at the vent (cf. Gudmunsson et al., 2016, Coppola et al., 2017, Dirsherl and Rossi., 2018).

295

296

4. Eruptive trend derived from satellite thermal data

298 One of the most significant feature of this eruption was the overall exponential trend of the satellite-

299 derived cumulative volume (Fig. 3b). As outlined by recent studies, this trend mirrors almost perfectly

300 the slow subsidence of the Bárðarbunga caldera floor (Fig. 3b) and suggests a strong connection

301 between source caldera/reservoir dynamic, and the eruptive dynamics 45 km distant (Gudmundsson

et al., 2016; Coppola et al., 2017). According to these works, the exponential decay of effusion rates was driven by a decrease of magma-static pressure, associated to the shrinking of the magma chamber and the gravity-driven collapse of Bárðarbunga caldera. In this scenario, the instantaneous effusion rate at the vent follows a perfectly exponential curve (blue line in Fig 4a) that has been used as a benchmark for our MODIS-derived *TADRs'* (red line in Fig 4a). Hence, the residuals between the two rates (observed - modeled; Fig. 4b) enhance temporary variations of the source process, or instabilities of the thermal proxy due to lava flow emplacement dynamic. In the following section, we discuss the effusive trend in the light of the evolving emplacement style observed in the Holuhraun lava field.

According to Pedersen et al. (2017) the Holuhraun eruption can be subdivided in three main phases, characterized by evolving lava transport processes.

The phase 1 (*31 August – 12 October 2014*) was characterized by lava transport confined to *open channels* that led the formation of four consecutive lava flows emplaced side by side (no. 1–4 in Fig 4b). During this phase the discharge rates measured on the field were comprised between 350 and 100 m^3 s^{-1} (Pedersen et al., 2017), in good agreement with satellite-derived values. The four flow units reached distances of 16.9, 11.8, 16.3 and 11.0 km, respectively (Fig. 4a), and covered a total area of 58.31 km^2 (Pedersen et al., 2017). Given a flow field volume of 0.78 km^3 estimated on October 12 (Fig. 3b), the mean flow thickness characterizing the Phase 1 was 13.4 m, consistent with the thickness of each single flow units observed on the field (Pedersen et al., 2017). During this period our *TADRs* measurements show the greatest oscillations around the modelled value (up to ± 60%), resulting in sharp variations exactly in correspondence of the activations of the distinct flow units (Fig 4b).
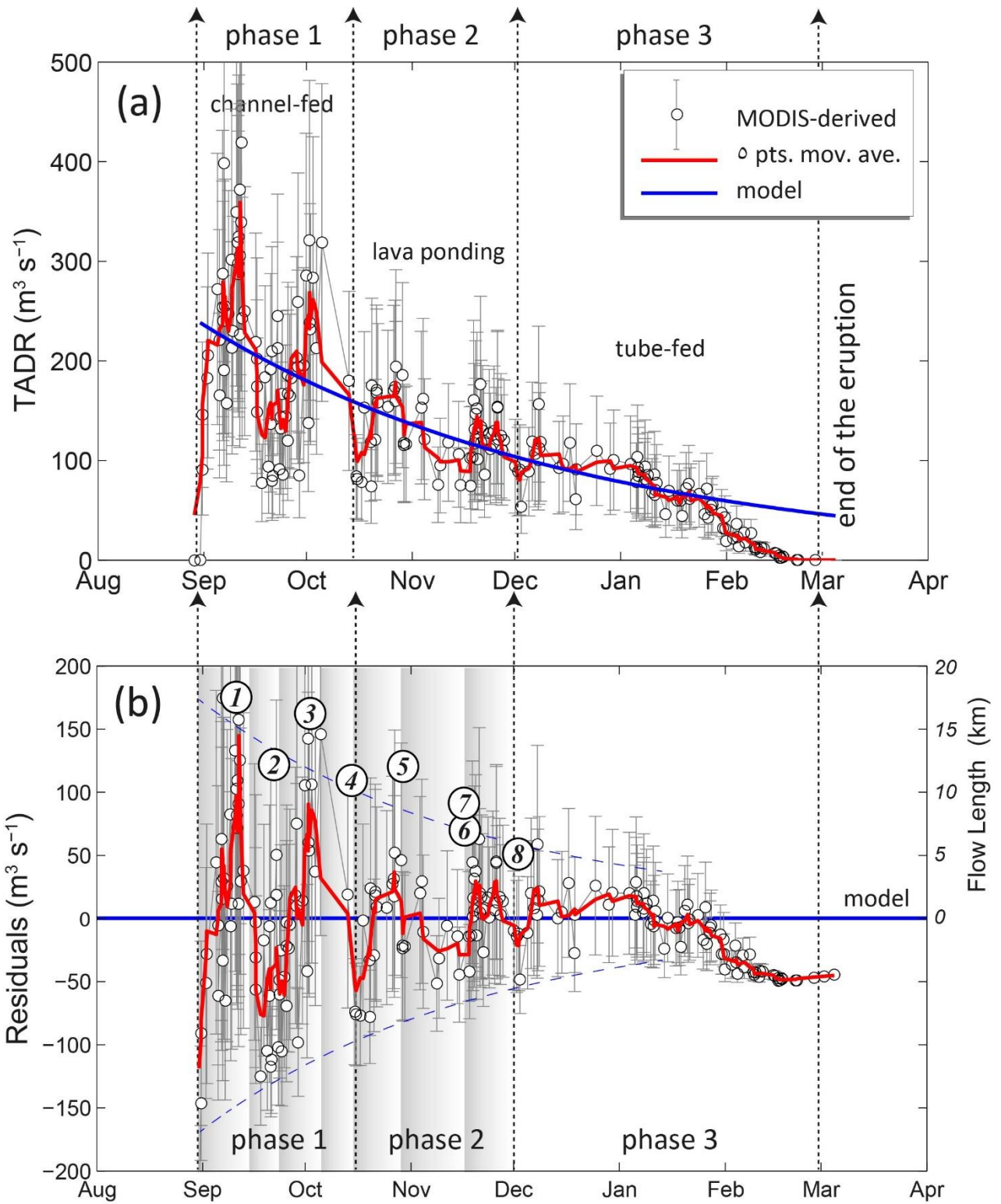
Figure 4. (a) *TADR* derived from MIROVA data (white circles) by using the radiant density approach (eqs. 5 and 6). The

blue line represents the best-fit exponential model (Coppola et al., 2017) hereby considered the real effusion rate at the

vent. (b) Residuals flow rates (left axis) obtained by subtracting the model from the observations (i.e. MODIS-derived

TADR minus modelled effusion rates). Note how the residuals oscillate around the model showing a decreasing amplitude

through time. The timing and amplitude of the residual pulses are coherent with the occurrence and maximum length of

the main channel-fed flow units numbered from 1 to 8 (data from Pedersen et al., 2017). The three phase of the eruption

described by Pedersen et al., 2017 are also shown.

The phase 2 (*13 October – 30 November 2014*) had lower effusion rates (150 – 100 m^3 s^{-1}) and was

characterized by the formation of a < 1km^2 lava pond, that acted as a distributor of subsequent lava

flows (i.e. flows no. 5–8; Pedersen et al., 2017). These flow units reached gradually shorter distances

(11.7, 8.4, 7.1, 5.4 km, respectively) and were accompanied by satellite-derived TADRs showing

decreasing oscillation amplitudes (Fig. 4b). Towards the end of this phase the occurrence of *inflation*

plateaus provided the first evidences of a growing lava tube system, with satellite-derived TADRs

becoming more stable (Fig. 5b). About 0.52 km^3, of lava was erupted during this phase (Fig. 3a)

producing a net increment of the flow field area of 18.7 km^2 (Pedersen et al., 2017). By the end of

November the flow field reached an average thickness of 16.9 m.

During the third phase (*1 December 2014 – 27 February 2015*) the lava transport was mainly confined

to *lava tubes* which fed several breakouts and inflation plateaus along the initial flow units no. 1 and

2 (Pedersen et al., 2017). More than 19 km^2 of the flow field was resurfaced, with discharge rates

much more steady (±20%) and typically lower than 100 m^{3}s^{-1}. A sharp reduction of TADR was

recorded since 27 January 2015 and preluded the end of the eruption occurred one month later, on the

27 February 2015 (Fig.4). This reduction was interpreted by Coppola et al., (2017) as due to the

gradual closure of the magma path once the overpressure inside the dike had dropped below a critical

value. The lava tube system distributed about 0.4 km^3 during this phase, with the lava field reaching

a final extension of 85.4 km^2. The inflation and resurfacing processes that operated through the tube

system led the average flow thickness to increase up to 20.2 m.

The emplacement of the major lava flows (phases 1 and 2) is outlined by the occurrence of apparent

TADR's "pulses" (Fig. 4a) oscillating around the modelled value for effusion rate (Fig. 4b). Pulsating

effusive activity has been recognized at several basaltic volcanoes and may results from different

processes such as pulsed magma supply, repeated accumulation and collapse of a foam layer at the reservoir roof, or by processes of magma mixing occurring within the magma chamber (e.g., Harris and Neri 2002, Lautze et al., 2004). However, in the case of Holuhraun eruption, the link between the effusive trend and the collapse of the caldera (Fig. 3b) claims for a simple, gravity-driven dynamic (Gudmundsson et al., 2016; Coppola et al., 2017) that would exclude, or minimize, the occurrence of above mentioned processes. Hence, the *TADR*'s pattern overprinted to the exponential trend is likely related to the emplacement dynamic occurred during the course of the eruption, and especially during the phases 1 and 2. Laboratory experiments (Garel et al., 2012, 2014) and theoretical treatments (Tarquini 2017), demonstrated that a constant effusion rate can actually produce pulses of the radiative power (Fig. 4b) that reflect the non-equilibrium steady-state growth of compound lava flow fields. According to Tarquini (2017) each flow unit will advance until the thermal equilibrium will be reached and the flow front stop. Hence, the system is resettled to give origin to a new flow unit. This seems to be exactly the dynamic occurred during the emplacement of the Holuhraun lava field, in which each apparent *TADR's* pulse correlates with a phase of lengthening of a distinct flow unit. Notably, the amplitude of the pulses decreased with time as the overall effusion rate declined, the maximum length attained by the flow units reduced, and the emplacement style evolved from channel- to tube-fed (Fig. 4b).


5. Evolving emplacement style, evolving thermal structure

In this section, we illustrate how the evolving emplacement style and the channel- to tube-fed transition affected the surface thermal structure of the Holuhraun's lava field. In particular, we used the temperature profiles (as the one shown in Fig. 1c) obtained from the MODIS image, in order to track the position of the active flow fronts and all the hot lava surfaces emerging along the principal flow path (from West to East). By stacking together all the W-E profiles the presence of active lavas (i.e. the vent(s), open-channel(s), breakout(s), flow front(s), etc.) appears as high-temperature features

382 (pixels), whose intensity, contiguity and extension can be easily visualized as shown in Fig. 5a. We

383 assumed that the position of the flow front is represented by the easternmost pixel having a brightness

384 temperature (BT4) of 50°C higher than the background (white dashed line in Fig. 5a). Hence, the

385 distance between this pixel and the one located over the active vent (Fig. 1b), provides a measurement

386 of the active flow length at each satellite overpass (red line in Fig. 5b). Lava flow lengths measured

387 on the field during the phases 1 and 2 (Flows no. 1 to 8) are also plotted for comparison (Fig. 5b).

388 This analysis indicates that during the phases 1 and 2, the active flow fronts were thermally connected

389 to the vents, through a high-radiating feature representing the open channels. On the other hand, since

390 December 2014 the reduction of lava discharge rate caused a marked shortening of the open channels,

391 although the lava field was still characterized by the presence of active lavas at the distal front(s).

392 Notably, between the two hot, active zones (i.e. open channels and flow front) there low-temperature

393 zone corresponding to crusted and cooling lava surfaces (Fig. 5a). This is a clear thermal evidence

394 that since the beginning of the phase 3 the transport of lava occurred along a master tube system and

395 that the emplacement style started to be *tube-fed* dominated.
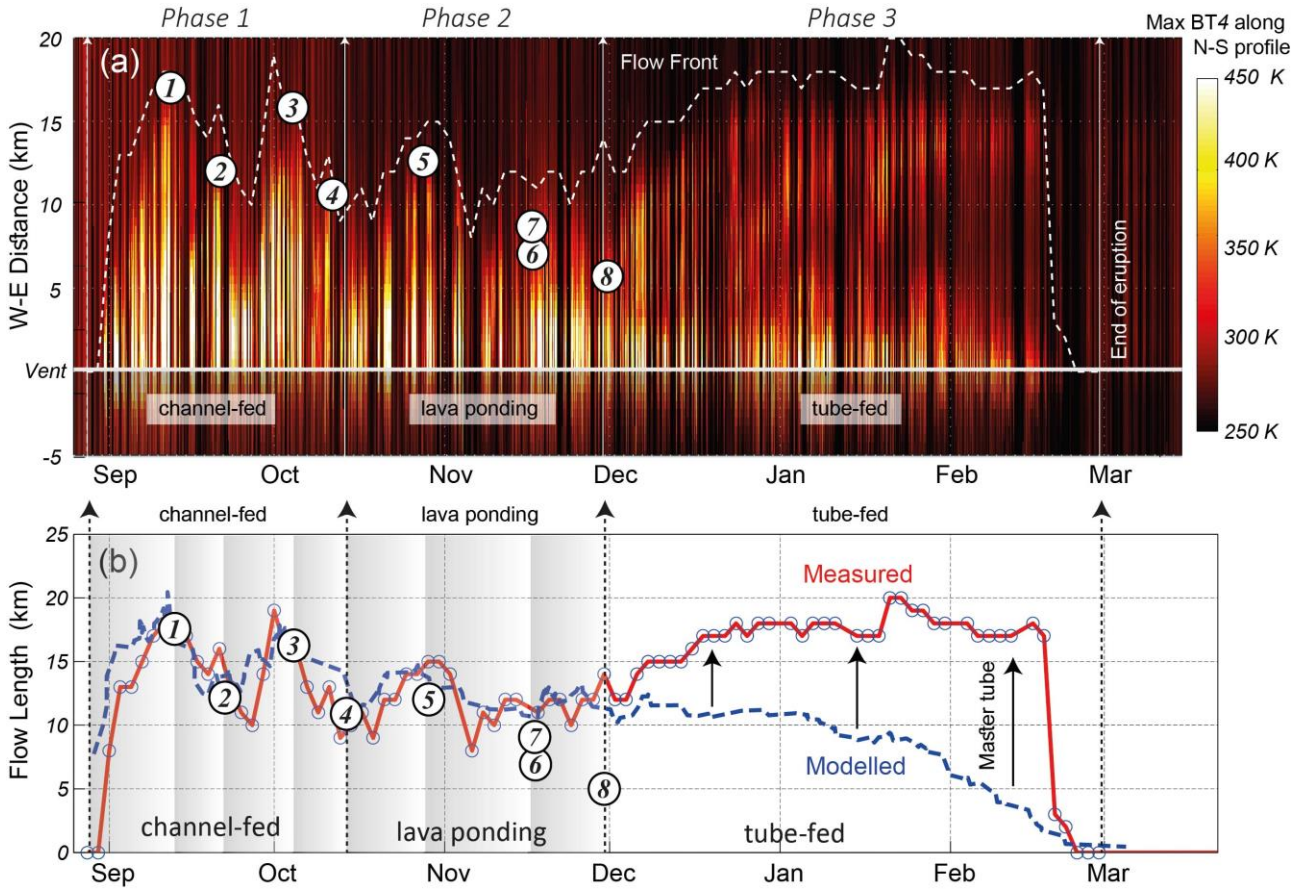
Figure 5. (a) Evolution of the along-path thermal structure of the Holuhraun lava flow. This plot is obtained by stacking together all the thermal profiles (max BT4 along each N-S line) as those illustrated in Fig. 1c. The white dashed line indicate the position of the active flow front (see the text for details); (b) Comparison between measured (red dashed line) and modelled (blue line) flow length. The Calvari & Pinkerton's model (eq. 7) assumes emplacement style dominated by *channel-fed*, cooling limited conditions. The discrepancy between measured and modelled flow distance after December 2014 outline the increasing efficiency of *tube-fed* emplacement style in transporting the lava to the flow front.

As a pure theoretical exercise, the flow extension measured by using the temperature profiles has been compared (Fig. 5b) with the maximum distance (L_{max}) predicted by one of the simplest empirical model developed for single, cooling-limited, channel-fed lava flow (cf. Walker 1973; Harris and Rowland, 2009). In particular, we used the Calvari and Pinkerton's equation (1998) that takes into account exclusively the *TADRs* measurements for the estimation of flow length:

$$L_{max} = 10^{3.11} \times (TADR)^{0.47} \qquad \text{(eq.7)}$$

411   The coefficients of equation 7 were empirically determined by regression analysis of single channel-

412   fed Etnean lava flows lasting 1 to 12 days, a duration very similar to the single flow units observed

413   at Holuhraun. This model does not require any knowledge of several others parameters (i.e.

414   underlying slope, lava temperature, viscosity, velocity, channel width, channel depth, etc…) that are

415   necessary to predict flow length using other approaches (see Harris and Rowland 2009 for a review),

416   but that are difficult, if not impossible to be constrained for each flow unit. However, despite its

417   simplicity, this empirical model of Calvari and Pinkerton 1998 allows to calculate the maximum

418   length of the Holuhraun's lava flow, and to see the effects of an emplacement style persistently

419   dominated by channel-fed, cooling-limited conditions (blue line in Fig. 5b).

420   During the phases 1 and 2, there is an excellent correlation between the measured and the modelled

421   flow lengths, both in terms of absolute values and pattern (Fig. 5b). This corroborate the fact that

422   during this period the emplacement style was effectively those for which eq.7 was proposed to

423   describe, that is single, channel-fed flows. Differently, since December 2014, there is a growing

424   discrepancy between the measured and modelled flow length (Fig. 5b), exactly in correspondence of

425   the formation of a master lava tube, as observed in the field (Pedersen et al., 2017).

426   From this picture, it is clear that the lower discharge rates characterizing the Phase 3, did not affect

427   the maximum extent of the lava flow, still reaching a distance of more than 15 km, just before the end

428   of the eruption (Fig. 5b). By paraphrasing Harris and Rowland, (2009) "the transition from poorly

429   insulated (*channel-fed*) to well insulated (*tube-fed*) regimes increases the length that a lava flow can

430   extend for a given *TADR*".

431   Notably, we may calculate the radiant density (c_{rad}= *VRE/Vol*) typical of the tube-fed flow field, by

432   dividing the thermal energy measured during the Phase 3 (*VRE* = ~ 0.4×10^{17} J; Fig. 2b) by the

433   volume lava erupted in the same time window, derived from Tandem-X measurements (*Vol* = $2.6 \times$

434   10^8 m³; Fig. 3a; Dirscherl and Rossi 2018). The resulting radiant density (c_{rad} = ~1.5×10^8 J m⁻³) is

435   only slightly higher than the radiant density calculated in the same way for the bulk channel-fed flow

436   field emplaced during phases 1 and 2 (c_{rad} = ~1.1×10^8 J m⁻³). This suggests that the variation of the

emplacement style produces an uncertainty in the *TADRs* measurement that does not exceed 30%, when provided in near real time. In other words, our results point out that, the formation of a lava tube does not affect substantially the amount of "active" lava radiating to the atmosphere, but simply "made this lava to be transported further from the vent". The lava tube thus act as a simple extension of the volcanic conduit, by displacing the vent downstream, likely along the main axis of the previously formed flow units. The recognition of this behavior in near real time allow to update the vent location and has been proved to be a necessary improvement to correct estimation of the lava flow path and the effective runout distance (Harris et al., 2018, this issue).

6. *Operational use of MIROVA system during the effusive crisis*

By the end of November 2014, MIROVA started to be part of the monitoring system operative at the Icelandic Meteorological Office (IMO) with the coverage of nine active volcanic systems. IMO is the main institution in Iceland in charge of monitoring natural hazards and issuing forecast and warnings in case of impending or on-going eruptions. It operates a multi-sensors network that includes seismometers, GPS and gas sensors for the geophysical monitoring. During the Holuhraun eruption, gas monitoring activity was improved and new instrumentations were deployed and maintained at the eruption site for the entire duration of the event (Pfeffer et al. 2017). The MIROVA system showed its strength and reliability in a period of the year when, in Iceland, the day light time is very short. Several of the instrumentations and products that could normally be used to monitor an eruption, started to fail or to give incomplete data sets due to harsh weather conditions and limited sunlight. MIROVA provided a robust and continuous data set on a daily basis which was used from November to March to follow the health and strength of the eruption, as well as the post-eruption phase.

On the operative side this system is revealed to be an important monitoring tool for following the temporal evolution of the eruption and providing estimates of the erupted lava volume in near real time (Coppola et al., 2017). Extrapolation of the effusive trend during the ongoing eruption may in

fact be used to forecast total erupted lava volume, which in turn is fundamental to drive some lava flow modelling (i.e. Tarquini et al., 2018). Also, the recognition of emplacement style through the analysis of flow' surface thermal structure (i.e. channel- or tube-fed lava flows) can be used to update the position of active flow fronts, and to choose the appropriate modeling strategy, by tuning some appropriate parameters that govern lava flow simulation's codes (i.e. Tarquini et al., 2018, this issue). Most importantly the thermal data have proved to be very important for constraining the time of the eruption end. A drastic change of *TADR* was observed since the end of January 2015 becoming clear the second week of February 2015 (Fig. 4a). This change was interpreted by Coppola et al. (2017) as due to the gradual closure of the magma path (dike) and indicated the potential timing of the end of the eruption in quite a good advance, about one month before the declaration of ceased eruption. These data were discussed within the Scientific Board Management meetings that were held from the beginning of the eruption in collaboration with the Icelandic Civil Protection and the University of Iceland. The very low TADR detected on 26 February 2017 (0.2 m^3 s^{-1}; Fig. 4a), supported the decision for a field crew to flight over the eruptive site on February 27 and declare that the eruption was over.

The thermal data were useful for providing a semi-quantitative indication of the strength of the gas source affecting the ground level concentration (Simmons et al., 2017). Due to its extension the lava field itself was a considerable source of volcanic gases. In addition, the gas released close to the surface was more easily trapped within the boundary layer and largely affected the concentration at ground. This fact suggested that the MIROVA detection and the *VRP* temporal variation could be correlated with the amount of gases released at the source. In this way the *VRP* data have been used by the forecasters at IMO to identify, in a qualitative way, when to expect an increase in the SO_2 values in areas located downwind the eruption site.

7. Conclusions

During the 2014-2015 Bárðarbunga-Holuhraun eruptive crisis, one of the main challenge for the volcanological community was to monitor the effusive process in a safely, timely and routinely manner. For the whole duration of the eruption, MIROVA provided a robust and continuous set of thermal data that were used to depict the effusive trend and to estimates the erupted lava volume although the changing emplacement conditions (from channel- to tube-fed flow) introduced uncertainties in the interpretation of the data.

The retrospective analysis of this eruption provides an exceptional opportunity to study the relationship between heat flux and *TADR* during the emplacement of a large compound lava field. We show that the overall trend of thermal emission was related to the combined effect of two over imposed patterns: (i) a main exponential decay of the effusion rate trend, governed by the source processes and (ii) a secondary pulsating pattern related to the emplacement dynamic of the flow field. We found that the magnitude and timing of these pulses were strictly related to the timing and length scales of discrete flow units characterizing open-channel lava transport. Conversely, the formation of lava tubes produces smaller instabilities and promotes lava to flow at greater distance in steady-state thermal conditions. This process is clearly visible from the evolution of the thermal structure depicted from the MODIS-MIROVA images and allow to track changes in the *lava transport mechanisms* operating during the eruption (Fig. 5a). The results presented here clearly indicate that the calculation of erupted lava volumes from the integration of satellite-derived *TADR* allow to smooth the short-term perturbation associated to the emplacement dynamic and provide a robust way to depict source eruptive trends. We thus regard the application of this methodology as a key-factor in volcano monitoring and satellite-data-driven response to an effusive crisis (Harris et al., 2018).

References

Bonny, E., T. Thordarson, R. Wright, A. Höskuldsson, I. Jónsdóttir (2018) The volume of lava erupted during the 2014 to 2015 eruption at Holuhraun, Iceland: A comparison between satellite and ground-based measurements, J Geophys Res Solid Earth, 123. https://doi.org/10.1029/2017JB015008.

Calvari, S. and H. Pinkerton (1998) Formation of lava tubes and extensive flow field during the 1991–1993 eruption of Mount Etna, J. Geophys Res, B103, 27291–27301.

Coppola, D., M. Laiolo, D. Piscopo and C. Cigolini (2013) Rheological control on the radiant density of active lava flows and domes, J. Volcanol. Geotherm. Res., 249, 39–48. doi:10.1016/j.jvolgeores.2012.09.005.C.

Coppola, D., M. Laiolo, C. Cigolini, D. Delle Donne and M. Ripepe (2016) Enhanced volcanic hot-spot detection using MODIS IR data: Results from the MIROVA system, in Harris A. J. L. , T. De Groeve, F. Garel and S. A. Carn (eds.) Detecting, Modelling, and Responding to Effusive Eruptions, Geological Society, London, Sp. Pub. 426, p. 181–205, doi:10.1144/SP426.5.

Coppola, D., M. Ripepe, M. Laiolo and C. Cigolini (2017) Modelling Satellite-derived magma discharge to explain caldera collapse, Geology 45(6), 523-526. doi:10.1130/G38866.1.

Crisp, J. and S. Baloga (1990) A method for estimating eruption rates of planetary lava flows, Icarus, 85(2), 512-515.

Crisp, J. and S. Baloga (1990) A model for lava flows with two thermal components, J. Geophys. Res., 95 (B2), 1255-1270.

Dirsherl, M. and C. Rossi (2018) Geomorphometric analysis of the 2014–2015 Bárðarbunga volcanic

538   eruption, Iceland, Remote Sens. Environ, 204, 244-259.

539 Dragoni, M. and A. Tallarico (2009), Assumptions in the evaluation of lava effusion rates from heat

540   radiation, Geophys. Res. Lett., 36, L08302. doi:10.1029/2009GL037411.

541 Garel, F., E. Kaminski, S. Tait and A. Limare (2012) An experimental study of the surface thermal

542   signature of hot subaerial isoviscous gravity currents: implications for thermal monitoring of

543   lava flows and domes, J. Geophys. Res. 117:B02205. doi: 10.1029/2011JB008698.

544 Garel, F., E. Kaminski, S. Tait and A. Limare (2014) An analogue study of the influence of

545   solidification on the advance and surface thermal signature of lava flows, Earth Planet. Sci.

546   Lett., 396, 46–55.

547 Garel, F., E. Kaminski, S. Tait and A. Limare (2015) A fluid dynamics perspective on the

548   interpretation of the surface thermal signal of lava flows, , in Harris A. J. L. , T. De Groeve, F.

549   Garel and S. A. Carn (eds.) Detecting, Modelling, and Responding to Effusive Eruptions,

550   Geological Society, London, Sp. Pub. 426, 243-256.doi: 10.1144/SP426.6

551 Gíslason, S. R., G. Stefánsdóttir, M. A. Pfeffer, S. Barsotti, Th. Jóhannsson, I.Galeczka, E. Bali, O.

552   Sigmarsson, A. Stefánsson, N. S. Keller, A. Sigurdsson, B. Bergsson, B. Galle, V. C. Jacobo,

553   S. Arellano, A. Aiuppa, E. B. Jónasdóttir, E. S. Eiríksdóttir, S. Jakobsson, G. H. Guðfinnsson,

554   S. A. Halldórsson, H. Gunnarsson, B. Haddadi, I. Jónsdóttir, Th. Thordarson, M. Riishuus, Th.

555   Högnadóttir, T. Dürig, G. B. M. Pedersen, A. Höskuldsson and M. T. Gudmundsson (2015)

556   Environmental pressure from the 2014–15 eruption of Bárðarbunga volcano, Iceland,

557   Geochem. Persp. Lett., 1, 84-93.

558 Gudmundsson, A., N. Lecoeur, N. Mohajeri and T. Thordarson (2014) Dike emplacement at

559   Bárðarbunga, Iceland, induces unusual stress changes, caldera deformation, and earthquakes,

560   Bull. Volcanol., 76, 869–875. doi:10.1007/s00445-014-0869-8.

561 Gudmundsson, M. T., K. Jónsdóttir, A. Hooper, E. P. Holohan, S. A. Halldórsson, B. G. Ófeigsson,

562   S. Cesca, K. S. Vogfjörd, F. Sigmundsson, T. Högnadóttir, P. Einarsson, O. Sigmarsson, A. H.

563   Jarosch, K. Jónasson, E. Magnússon, S. Hreinsdóttir, M. Bagnardi, M. M. Parks, V.

564   Hjörleifsdóttir, F. Pálsson, T. R. Walter, M. P. Schöpfer, S. Heimann, H. Reynolds, S. Dumont,

565   E. Bali, G. H. Gudfinnsson, T. Dahm, M. J. Roberts, M. Hensch, J. M. Belart, K. Spaans, S.

566   Jakobsson, G. B. Gudmundsson, H. M. Fridriksdóttir, V. Drouin, T. Dürig, G. Aðalgeirsdóttir,

567   M. S. Riishuus, G. B. Pedersen, T. van Boeckel, B. Oddsson, M. A. Pfeffer, S. Barsotti, B.

568   Bergsson, A. Donovan, M. R. Burton, A. Aiuppa (2016) Gradual caldera collapse at

569   Bárdarbunga volcano, Iceland, regulated by lateral magma outflow, Science, 353.

570   doi:10.1126/science.aaf8988.

571 Harris, A. J. L. and M. Neri (2002) Volumetric observations during paroxysmal eruptions at Mount

572   Etna: Pressurized drainage of a shallow chamber or pulsed supply?, J. Volcanol. Geotherm.

573   Res., 116, 79–95, doi:10.1016/S0377-0273(02)00212-3.

574 Harris, A. J. L. and S. Baloga (2009) Lava discharge rates from satellite-measured heat flux, Geophys.

575   Res. Lett., 36, L19302. doi:10.1029/2009GL039717.

576 Harris, A. J. L. and S. K. Rowland (2009) Effusion rate controls on lava flow length and the role of

577   heat loss; a review, in Thordarson, T., S. Self, G. Larsen, S. K. Rowland and A. Hoskuldsson

578   (eds) Studies in Volcanology: The Legacy of George Walker. Geological Society, London Sp.

579   Pub. of IAVCEI, 2, 33– 51.

580 Harris, A. J. L., S. Blake, D. A. Rothery, and N. F. Stevens (1997) A chronology of the 1991 to 1993

581   Etna eruption using AVHRR data: Implications for real time thermal volcano monitoring, J.

582   Geophys. Res., 102(B4), 7985–8003, doi:10.1029/96JB03388.

583 Harris, A. J. L., J. Dehn, and S. Calvari (2007) Lava effusion rate definition and measurement: A

584   review, Bull. Volcanol., 70, 1–22. doi:10.100 7/s00445-007-0120-y.

585 Harris, A. J. L., S. Carn, J. Dehn, C. Del Negro, G. Guðmundsson, B. Cordonnier, T. Barnie, S.

586   Calvari, T. Catry, T. de Groeve, D. Coppola, A. Davies, M. Favalli, E. Fujita, G. Ganci, F.

587   Garel, J. Kauahikaua, K. Kelfoun, V. Lombardo, G. Macedonio, J. Pacheco, M. Patrick, N.

588   Pergola, M. Ramsey, R. Rongo, K. Smith, S. Tarquini, T. Thordarson, N. Villenueve, P.

589   Webley, R. Wright and K. Zakzek (2016a) Conclusion: Recommendations and findings of the

590   RED SEED working group, in Harris A. J. L., T. De Groeve, F. Garel and S. A. Carn (eds.)

591   Detecting, Modelling, and Responding to Effusive Eruptions, Geological Society, London, Sp.

592   Pub. 426, p. 567-648. doi:10.1144/SP426.11.

593 Harris, A. J. L., T. De Groeve, S. Carn, F. Garel (2016b) Risk evaluation, detection and simulation

594   during effusive eruption disasters, in Harris A. J. L., T. De Groeve, F. Garel and S. A. Carn

595   (eds.) Detecting, Modelling, and Responding to Effusive Eruptions, Geological Society,

596   London, Sp. Pub. 426, p. 1-22. doi:10.1144/SP426.29.

597 Harris, A. J. L., O.M. Chevrel, D. Coppola, M.S. Ramsey, A. Hrysiewicz, S. Thivet, N. Villeneuve,

598   M. Favalli, A. Peltier, P. Kowalski, A Di Muro, J-L Froger, L. Gurioli (2018) Validation of

599   an integrated satellite-data-driven response to an effusive crisis: 2 the April–May 2018 eruption

600   of Piton de la Fournaise, Special Issue: MeMoVolc, Annals of Geophysics, (in press, this issue)

601 Lautze, N. C., A. J. L. Harris, J. E. Bailey, M. Ripepe, S. Calvari, J. Dehn, S. Rowland, and K. Evans-

602   Jones (2004) Pulsed lava effusion at Mount Etna during 2001, J. Volcanol. Geotherm. Res.,

603   137, 231–246. doi:10.1016/j. jvolgeores.2004.05.018

604 Pedersen, G. B. M., A. Höskuldsson, T. Dürig, T. Thordarson, I. Jónsdóttir, M. S. Riishuus, B. V.

605   Óskarsson, S. Dumont, E. Magnusson, M. T. Gudmundsson, F. Sigmundsson, V. J. P. B.

606   Drouin, C. Gallagher, R. Askew, J. Gudnason, W. M. Moreland, P. Nikkola, H. I. Reynolds, J.

607   Schmith and the IES eruption team (2017). Lava field evolution and emplacement dynamics of

608   the 2014–2015 basaltic fissure eruption at Holuhraun, Iceland, J. Volcanol. Geotherm. Res.,

609   10.1016/j.jvolgeores.2017.02.027.

610 Pfeffer, M. A., B. Bergsson; S. Barsotti; G. Stefánsdóttir; B. Galle, S. Arellano, V. Conde, A.

611   Donovan, E. Ilyinskaya, M. Burton, A. Aiuppa, R. C. W. Whitty, I. C. Simmons, Þ. Arason, E.

612   B. Jónasdóttir, N. S. Keller, R. F. Yeo, H. Arngrímsson, Þ. Jóhannsson, M. K. Butwin, R. A.

613   Askew, S. Dumont, S. von Löwis, Þ. Ingvarsson, A. La Spina, H. Thomas, F. Prata, F. Grassa,

614   G. Giudice, A. Stefánsson, F. Marzano, M. Montopoli and L. Mereu (2017) Ground-Based

615   Measurements of the 2014–2015 Holuhraun Volcanic Cloud (Iceland), Geosciences,8, 29.

616 Pieri, D. and S. M. Baloga (1986) Eruption rate, area, and length relationships for some Hawaiian

617   lava flows, J. Volcanol. Geotherm. Res., 30 (1), 29-45.

618 Ramsey, M. and A. J. L. Harris (2013) Volcanology 2020: How will thermal remote sensing of

619   volcanic surface activity evolve over the next decade? J. Volcanol. Geotherm. Res., 249, 217-

620   233.

621 Sigmundsson, F., A. Hooper, S. Hreinsdóttir, K. S. Vogfjörd, B. G. Ófeigsson, E. R. Heimisson, S.

622   Dumont, M. Parks, K. Spaans, G. B. Gudmundsson, V. Drouin, T. Árnadóttir, K. Jónsdóttir, M.

623   T. Gudmundsson, T. Högnadóttir, H. M. Fridriksdóttir, M. Hensch, P. Einarsson, E.

624   Magnússon, S. Samsonov, B. Brandsdóttir, R. S. White, T. Ágústsdóttir, T. Greenfield, R. G.

625   Green, A. R. Hjartardóttir, R. Pedersen, R. A. Bennett, H. Geirsson, P. C. La Femina, H.

626   Björnsson, F. Pálsson, E. Sturkell, C. J. Bean, M. Möllhoff, A. K. Braiden and E. P. S. Eibl

627   (2015) Segmented lateral dyke growth in a rifting event at Bárðarbunga volcanic system,

628   Iceland, Nature, 517, 191–195.

629 Sigurðsson, H. and R. S. J. Sparks (1978) Rifting episode in North Iceland in 1874–1875 and the

630   eruptions of Askja and Sveinagja, Bull. Volcanol., 41, 149–167.

631 Simmons, I, M. A. Pfeffer, E. Calder, B. Galle, S. Arellano, D. Coppola and S. Barsotti (2017)

632   Extended SO_2 outgassing from the 2014-2015 Holuhraun lava flow field, Iceland, Bull.

633   Volcanol., X. DOI: 10.1007/s00445-017-1160-6.

634 Tarquini, S. (2017) A review of mass and energy flow through a lava flow system: insights provided

635   from a non-equilibrium perspective, Bull. Volcanol., 79, 64. https://doi.org/10.1007/s00445-

636   017-1145-5.

637 Tarquini, S., M. de' Michieli Vitturi, E. Jensen, G. Pedersen, S. Barsotti, D. Coppola, M. A. Pfeffer

638   (2018) Modeling lava flow propagation over a flat landscape by using MrLavaLoba: the case

639   of the 2014–2015 eruption at Holuhraun, Iceland, Special Issue: MeMoVolc, Annals of

640   Geophysics, 61. https://doi.org/10.4401/ag-7812.

641   Walker, G. P. L. (1973) Lengths of lava flows. Philosophical Transactions of the Royal Society,

642   London, 274, 107–118.

643   Wooster, M. J., B. Zhukov and D. Oertel (2003) Fire radiative energy for quantitative study of

644   biomass burning: derivation from the BIRD experimental satellite and comparison to MODIS

645   fire products, Remote Sens. Environ., 86, 83–107. http://dx.doi.org/ 10.1016/S0034-

646   4257(03)00070-1.

647   Wright, R., S. Blake, A. J. L. Harris, and D. Rothery (2001) A simple explana-tion for the space-

648   based calculation of lava eruptions rates, Earth Planet. Sci. Lett., 192, 223 – 233.

649   doi:10.1016/S0012-821X(01)00443-5.

650